Fission yeast Rad26^{ATRIP} delays spindle-pole-body separation following interphase microtubule damage

Matthew Herring*, Nick Davenport*, Kendra Stephan, Shawna Campbell, Rebecca White, Jonathan Kark and Tom D. Wolkow‡

University of Colorado at Colorado Springs, Department of Biology, 1420 Austin Bluffs Parkway, Colorado Springs, CO 80918, USA

*These authors contributed equally to this work

‡Author for correspondence (twolkow@uccs.edu)

Accepted 8 February 2010
Journal of Cell Science 123, 1537-1545

doi:10.1242/jcs.049478

Summary

The conserved fission yeast protein Rad26^{ATRIP} preserves genomic stability by occupying central positions within DNA-structure checkpoint pathways. It is also required for proper cellular morphology, chromosome stability and following treatment with microtubule poisons. Here, we report that mutation of a putative nuclear export sequence in Rad26^{ATRIP} disrupted its cytoplasmic localization in untreated cells and conferred abnormal cellular morphology, minichromosome instability and sensitivity to microtubule poisons without affecting DNA-structure checkpoint signaling. This mutation also disrupted a delay to spindle-pole-body separation that occurred following microtubule damage in G_2. Together, these results demonstrate that Rad26^{ATRIP} participates in two genetically defined checkpoint pathways – one that responds to genomic damage and the other to microtubule damage. This response to microtubule damage delays spindle-pole-body separation and, in doing so, might preserve both cellular morphology and chromosome stability.

Key words: DNA structure checkpoint, Microtubule damage

Introduction

Prokaryotes and eukaryotes delay cell-cycle progression in response to DNA damage (Hartwell and Weinert, 1989; Opperman et al., 1999). In eukaryotes, DNA-structure checkpoints are required for these cell-cycle delays, which coordinate DNA repair with division (Weinert and Hartwell, 1988; Carr, 1995). As failure to repair DNA damage can lead to genetic instability and cancer (Hartwell, 1992; Weinert and Lydall, 1993; Weinert and Hartwell, 1988), these checkpoints might form barriers between precursor lesions and tumorigenesis (Bartkova et al., 2005).

Elegant yeast screens led to the discovery of mutants defining DNA-structure checkpoint proteins (Weinert and Hartwell, 1988; al-Khodairy and Carr, 1992; Rowley et al., 1992; Enoch et al., 1992; Walworth et al., 1993; al-Khodairy et al., 1994; Weinert and Hartwell, 1988; Weinert et al., 1994). These proteins participate in pathways composed of sensors and transducers that detect and transmit the presence of unreplicated and damaged DNA to the cell-cycle machinery (for reviews, see Kastan and Bartek, 2004; Rouse and Jackson, 2002b; Melo and Toczyski, 2002). The checkpoint sensor complexes detect abnormal DNA structures and/or processed lesions using parallel pathways. Following detection, physical assembly of these complexes somehow activates a PIKK (phosphoinositide 3-kinase related kinase) family member (Bonilla et al., 2008). PIKKs are evolutionarily related to phosphoinositide 3-kinases; members of both families share a highly conserved C-terminal kinase domain of ~300 residues that distinguishes them from all other eukaryotic kinases (Keith and Schreiber, 1995). Two PIKKs, called ataxia telangiectasia mutated (ATM) and ataxia telangiectasia and Rad3-related (ATR), are central to DNA checkpoint pathways in humans (for a review, see Abraham, 2001). Once activated by the sensor complexes, they phosphorylate downstream transducing kinases, including Chk1 and Chk2, which negatively regulate mitotic cyclin-dependent kinase.

It is becoming clear that these DNA-structure checkpoint pathways also influence spindle dynamics and cellular morphology. Crosstalk between the DNA-structure and spindle-assembly checkpoints was first observed in budding yeast, in which the checkpoints jointly mediate arrest during replication stress (Garber and Rine, 2002). Coordination between these pathways has now been observed in many eukaryotes and acts to sustain the anaphase delay following either genomic (Clemenson and Marsolier-Kergoat, 2006; Collura et al., 2005; Krishnan et al., 2004; Mikhailov et al., 2002) or microtubule stress (Zachos et al., 2007). These delays, which probably help to ensure proper chromosome segregation, might also be relevant during unperturbed division cycles that require extra time due to stochastic errors in kinetochore-microtubule attachment (for a review, see Zachos and Gillespie, 2007).

The altered morphology of *ataxia-telangiectasia* fibroblasts that carry primary lesions in ATM originally suggested that DNA checkpoint activity somehow influences morphology (McKinnon and Burgoyne, 1985). Studies with fission yeast, budding yeast and filamentous fungi confirm that this influence exists across evolution (Baschal et al., 2006; Malavazi et al., 2006; Enserink et al., 2006). It remains to be determined whether checkpoint proteins directly influence morphology by genetically defined pathways or whether morphological alterations arise as indirect consequences of the genetic instability that occurs following loss of DNA-structure checkpoints.

Fission yeast Rad3^{ATR} is a PIKK that is central to DNA-structure checkpoint signaling (Bentley et al., 1996). Rad3^{ATR} physically associates with Rad26^{ATRIP}, a regulatory subunit required for normal levels of Rad3 kinase activity (Edwards et al., 1999; Wolkow and Enoch, 2002). This Rad3-Rad26 checkpoint complex is conserved throughout evolution and exists in humans (ATR-ATRIP), budding yeast (MEC1-LCD1$^{DDC2/PIE1}$), *Xenopus* (xATR-xATRIP) and

possibly filamentous fungi (UvsB-UvsD) (Cortez et al., 2001; Rouse and Jackson, 2002a; Paciotti et al., 2000; Wakayama et al., 2001; De Souza et al., 1999).

Fission yeast Rad3 and Rad26 are also required when cells are challenged with the microtubule poisons methyl benzimidazole carbamate (carbendazim; MBC) and thiabendazole (TBZ) (Staron and Allard, 1964; Wolkow and Enoch, 2003; Baschal et al., 2006). This sensitivity is not caused by loss of DNA checkpoint activity, because checkpoint-deficient *hus1Δ* and *rad17Δ* cells exhibited wild-type growth on plates containing these drugs (Wolkow and Enoch, 2003). Furthermore, cytoplasmic Rad26-GFP accumulated during treatment with microtubule poisons, but not during treatment with genotoxins, suggesting that Rad26 responds specifically to microtubule damage (Baschal et al., 2006).

Here, we report the consequences of mutating a conserved putative nuclear export signal of Rad26^{ATRIP}. We observed that this mutation disrupts the localization of cytoplasmic Rad26^{ATRIP} in untreated cells and confers sensitivity to microtubule toxins but not genotoxins. These mutant cells also exhibit aberrant morphology, minor chromosome instability and a failure to delay spindle-pole-body separation during MBC treatment in G_2. Rad26 performs these functions independently of the spindle-assembly checkpoint protein Mad2. These results suggest that Rad26^{ATRIP} participates in a checkpoint response to microtubule damage in G_2 that delays entry into mitosis and, in doing so, might preserve both cellular morphology and chromosome stability.

Results

Rad26 and Mad2 respond to microtubule damage using different pathways

A benzimidazole-resistant α-tubulin allele (Yamamoto, 1980; Umesono et al., 1983) rescued the growth of *rad26Δ* cells on MBC (Fig. 1A), but not on the DNA-damaging agent phleomycin (Fig. 1A). We conclude that *rad26*$^+$ is required when microtubules are damaged.

The *mad2*-dependent spindle-assembly checkpoint delays exit from mitosis when microtubules are damaged (Li and Murray, 1991). Given that crosstalk between DNA-structure and spindle-assembly checkpoints exists, we hypothesized that *rad26*$^+$ might function to delay exit from mitosis during microtubule damage. Here, we investigated this hypothesis using a *nda3-311* cold-sensitive β-tubulin allele that blocks spindle formation and has

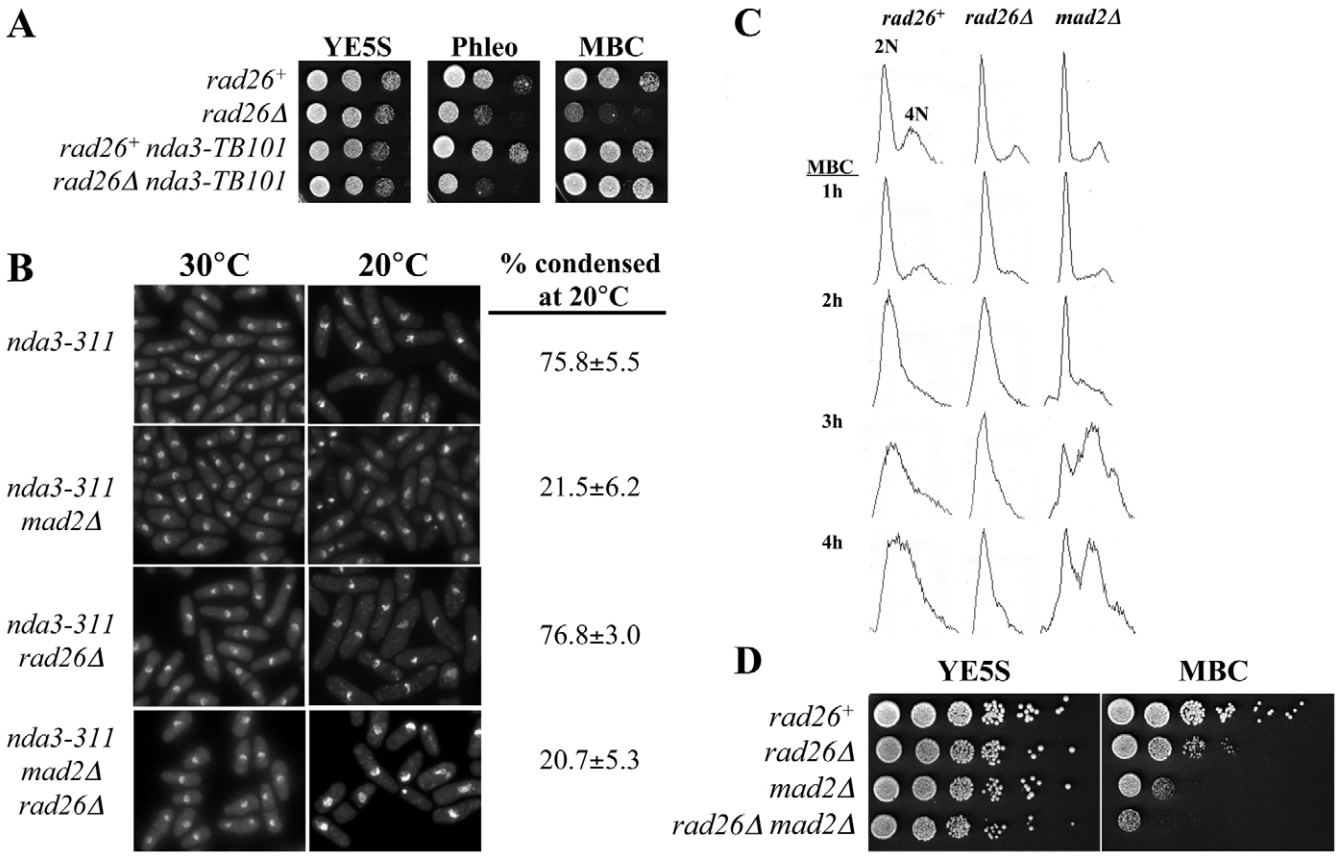

Fig. 1. The Rad26-dependent microtubule-stress response is not required for the spindle-assembly checkpoint. (**A**) *nda3-TB101* rescued the MBC sensitivity of *rad26Δ* cells. Cultures of *rad26*$^+$ (TE236), *rad26Δ* (TE257), *nda3-TB101* (TW1285) and *rad26Δ nda3-TB101* (TW1280) cells were used to perform plate assays (see Materials and Methods) on YE5S (complete medium), YE5S plus 0.125 μg/ml phleomycin and YE5S plus 8 μg/ml MBC. (**B**) Unlike *mad2Δ* cells, *rad26Δ* cells arrested with condensed chromatin in the *nad3-311* background. Cultures of *nad3-311* (TW1294), *nad3-311 rad26Δ* (TW1295), *nad3-311 mad2Δ* (TW1297) and *nad3-311 rad26Δ mad2Δ* (TW1301) were grown at 30°C in liquid YE5S to OD 0.3 before downshifting to 20°C for 5 hours. Cells were then fixed with cold methanol and stained with DAPI. (**C**) Unlike *mad2Δ* cells, *rad26Δ* cells delayed DNA replication in response to MBC treatment. Cultures of *rad26*$^+$ (TE236), *rad26Δ* (TE257) and *mad2Δ* (TW1219) were grown at 30°C in liquid YE5S to OD 0.3 before treating with 8 μg/ml MBC for four hours. Flow cytometry was performed using ethanol-fixed cells stained with Sytox green (see Materials and Methods). (**D**) The *rad26Δ mad2Δ* double mutant displayed an additive phenotype. Cultures of *rad26*$^+$ (TE236), *rad26Δ* (TE257), *mad2Δ* (TW1219) and *rad26Δ mad2Δ* (TW1286) cells were used to perform plate assays (see Materials and Methods) on YE5S and YE5S plus 6 μg/ml MBC.

been used to assay spindle-assembly checkpoint proficiency (Kanbe et al., 1990; He et al., 1997; Sczaniecka et al., 2008). When *nda3-311* cells are downshifted to 20°C, strains with an intact spindle-assembly checkpoint delay mitosis and accumulate condensed chromatin, whereas strains deficient in the spindle-assembly checkpoint progress through mitosis and into the next cell cycle. We found that 76% of *rad26*$^{+}$ and 77% of *rad26Δ* cells arrested with highly condensed nuclei following the downshift, compared to 22% of *mad2Δ* cells and 21% of *rad26Δmad2Δ* double-mutant cells (Fig. 1B). Therefore, *rad26*$^{+}$ does not participate in the *mad2*-dependent pathway that blocks exit from mitosis when microtubules are damaged in an *nda3-311* background.

We also tested whether *rad26*$^{+}$ is required to delay DNA replication during MBC treatment. For these experiments, flow cytometry was used to quantitate DNA in cells treated with 8 μg/ml MBC during a four-hour time course (Fig. 1C). The data show that *rad26*$^{+}$ and *rad26Δ* strains respond to MBC treatment by delaying further rounds of DNA replication. The same was not true for *mad2Δ* cells, which continued to replicate DNA despite the presence of MBC. Again, we observe that *rad26*$^{+}$ is not required in a *mad2*-dependent pathway.

We note that, whereas *rad26*$^{+}$ cells began to synthesize DNA and recover from MBC in the third hour of treatment, *rad26Δ* cells displayed a sharp arrest (Fig. 1C). This suggests that *rad26*$^{+}$ might be required to recover from microtubule stress; experiments to test this are underway.

If Rad26 and Mad2 perform different roles during microtubule damage, then the *rad26Δmad2Δ* double mutant should exhibit additive defects. Using plate assays, we observed that the *mad2Δ* allele conferred greater MBC sensitivity than the *rad26Δ* allele, whereas the *rad26Δmad2Δ* double mutant displayed an additive phenotype (Fig. 1D). We conclude that Rad26 and Mad2 participate in different pathways that, when disrupted, cause greater sensitivity to MBC than disruption of either pathway alone.

Rad26 has a putative nuclear export sequence

Our previous model suggested that cytoplasmic Rad26 participates in a response to microtubule damage (Baschal et al., 2006). Using the Minimotif Miner tool (Balla et al., 2006), we identified a cluster of hydrophobic residues near the C terminus of Rad26 that resembles a nuclear export sequence (NES) (Kutay and Guttinger, 2005). The ClustalW2 multiple sequence alignment tool (Larkin et al., 2007) revealed that the C-terminal location of this putative NES is conserved among homologous proteins in fission yeast, budding yeast, filamentous fungi and humans (Fig. 2A) (al-Khodairy et al., 1994; Wakayama et al., 2001; Paciotti et al., 2000; De Souza et al., 1999; Cortez et al., 2001). In a yeast two-hybrid screen for proteins with nuclear export activity, it was discovered that this region of Lcd1^{ATRIP} (referred to as YDR499W in the report) physically interacts with Crm1 and, when mutated (L670A or L673A), causes nuclear accumulation of GFP-Lcd1^{ATRIP} (Jensen et al., 2000). Together, these results suggest that this C-terminal motif is a bona fide NES in fission yeast Rad26^{ATRIP}.

The *rad26:4A* allele confers sensitivity to MBC

To test whether this conserved motif of Rad26 is required during microtubule damage, we changed four of the hydrophobic residues to alanines (Fig. 2A). The allele (*rad26:4A*) was then integrated into a *rad26Δ* strain, where its expression was driven by the endogenous *rad26*$^{+}$ genomic promoter. Plating assays were used to characterize the fitness of this strain during exposure to three different toxins (Fig. 2B). Phleomycin was used to induce DNA breaks (Sleigh and Grigg, 1977), hydroxyurea (HU) was used to stall replication forks (Zhao et al., 1998) and MBC was used to damage microtubules (Jacobs et al., 1988). The control dilutions in Fig. 2B show that the growth of *rad26Δ* cells was inhibited by all three toxins. Growth of the *rad26:4A* strain on HU and phleomycin was actually enhanced in comparison with the *rad26*$^{+}$ strain. However, *rad26:4A* growth was inhibited by MBC. Therefore, the *rad26:4A* allele specifically compromises growth on medium containing MBC.

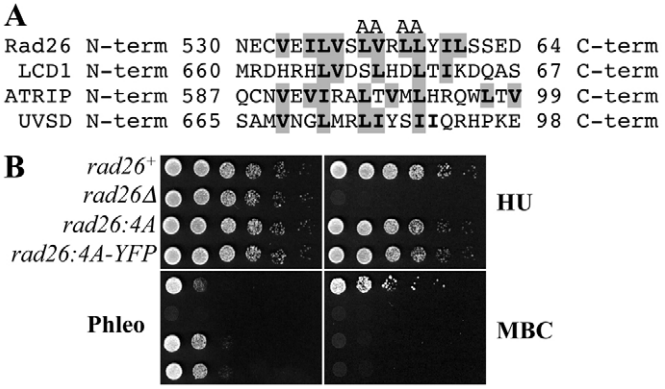

Fig. 2. The *rad26:4A* allele genetically separates the microtubule-stress response from the DNA checkpoint pathways. (**A**) Multiple sequence alignments of Rad26 homologs identified a conserved C-terminal motif that resembles an NES. Numbers indicate the location of this motif within each protein and the four 'A's above the alignment represent those hydrophobic residues that were changed to alanines in the Rad26:4A protein. (**B**) *rad26:4A* conferred sensitivity to MBC, but not HU or phleomycin. Cultures of *rad26*$^{+}$ (TE236), *rad26Δ* (TE257), *rad26:4A* (TW1275) and *rad26:4A-yfp* (TW1279) cells were used to perform plate assays (see Materials and Methods) on YE5S (complete medium), YE5S plus 5 mM HU, YE5S plus 0.125 μg/ml phleomycin and YE5S plus 8 μg/ml MBC.

Cytoplasmic localization of Rad26:4A-YFP is compromised in untreated cycling cells

If this conserved C-terminal motif functions as an NES, then the cytoplasmic localization of Rad26:4A should be affected. This was tested by tagging Rad26 and Rad26:4A with YFP, a tag that did not affect the growth characteristics of *rad26:4A* cells (Fig. 2B) or *rad26*$^{+}$ cells (data not shown). Whereas control experiments verified that Rad26-YFP localized to both the cytoplasm and nuclei of untreated cycling cells, we observed little Rad26:4A-YFP in the cytoplasm and an elevated signal in the nuclei (Fig. 3A). Fluorescence intensity measurements verified that the cytoplasmic Rad26:4A-YFP signal was weaker than the cytoplasmic Rad26-YFP signal, and that the nuclear Rad26:4A-YFP signal was stronger than the nuclear Rad26-YFP signal (Fig. 3B). Therefore, this conserved hydrophobic C-terminal motif is required for cytoplasmic localization of Rad26 in untreated cycling cells.

Rad26 accumulates in the cytoplasm following MBC treatment (Baschal et al., 2006). Here, we observed that both Rad26-YFP and Rad26:4A-YFP accumulate in the cytoplasm during MBC treatment (Fig. 3A). Therefore, this C-terminal motif is not required for cytoplasmic accumulation of Rad26 during MBC treatment, a response that might be directed by other putative NESs that appear in the Rad26 primary sequence (data not shown). That this response

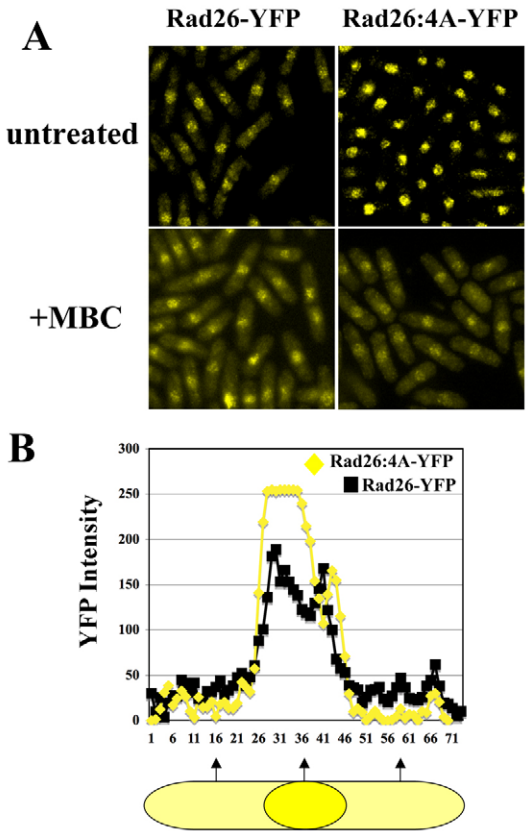

Fig. 3. Localization of Rad26:4A-YFP was compromised in untreated cycling cells. (**A**) Rad26:4A-YFP concentrated in the nucleus of untreated cells. Cultures of *rad26-yfp* (TW1234) and *rad26:4A-yfp* (TW1279) grown to OD 0.3 in liquid YE5S were untreated or treated with 8 μg/ml MBC for 1 hour. (**B**) Fluorescence intensity measurements convey the relative cytoplasmic and nuclear fluorescence found in untreated *rad26-yfp* and *rad26:4A-yfp* cells. ImageJ software (rsbweb.nih.gov/ij/) was used to map YFP intensity across the length of 50 *rad26-yfp* and 50 *rad26:4A-yfp* cells; average intensities are plotted.

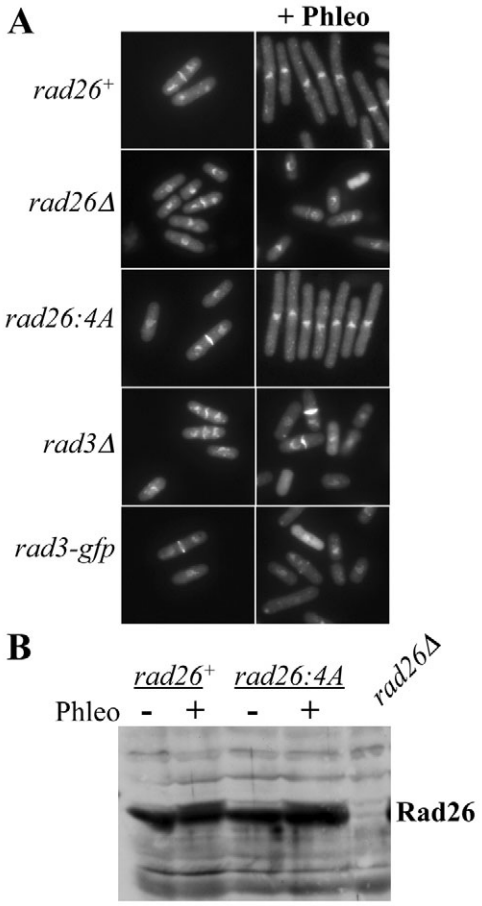

Fig. 4. The DNA-damage checkpoint of *rad26:4A* cells was intact. (**A**) *rad26:4A* cells undergo checkpoint arrest during phleomycin treatment. Cultures of *rad26*$^{+}$ (TE236), *rad26Δ* (TE257), *rad26:4A* (TW1275), *rad3Δ* (TE570) and *rad3-gfp* (TW1203) cells were split and either left untreated or treated with 7.5 μg/ml phleomycin for 3 hours before DAPI and calcofluor staining (Materials and Methods). (**B**) Phosphorylation of Rad26:4A occurred during phleomycin treatment. Cultures of *rad26*$^{+}$ (TE236), *rad26Δ* (TE257) and *rad26:4A* (TW1275) cells were split and either left untreated or treated with 7.5 μg/ml phleomycin for 3 hours. Cell extracts and western blots were prepared as described previously (Wolkow and Enoch, 2002).

occurs in *rad26:4A* cells only demonstrates that, in and of itself, cytoplasmic accumulation of Rad26 is not sufficient for a proper response to microtubule damage.

The DNA-damage checkpoint of *rad26:4A* cells is intact

Although the plate assays in Fig. 2B suggest that Rad26:4A functions normally in DNA checkpoint pathways, we used two more assays to test the possibility that it does not. First, liquid cultures treated with phleomycin were used to test whether *rad26:4A* cells exhibit a phenotypically normal checkpoint response. Control experiments showed that the DNA-damage checkpoint functions normally in *rad26*$^{+}$ and *rad26:4A* cells, which continued to elongate while restraining nuclear division and septation during phleomycin treatment (Fig. 4A). The *rad26Δ* cells displayed the classic checkpoint-defective phenotype (Enoch and Nurse, 1990) and progressed through mitosis and septation in the presence of phleomycin. Therefore, *rad26:4A* cells exhibit a phenotypically normal checkpoint response.

Rad3-dependent phosphorylation of Rad26 occurs during DNA-damage checkpoint activation and is used as a biochemical marker of checkpoint function (Edwards et al., 1999). To verify that the *rad26:4A* cells have a functional DNA-damage checkpoint, we tested whether Rad26:4A was phosphorylated during phleomycin treatment. Western blots showed that both Rad26 and Rad26:4A were expressed at very similar levels and phosphorylated during phleomycin treatment (Fig. 4B). We conclude that the DNA-damage checkpoint functions properly in the *rad26:4A* background.

The *rad3-gfp* allele also genetically separates the microtubule-damage response from the DNA-structure checkpoint response

In the course of these studies, we observed that the growth of *rad3-gfp* cells was compromised on phleomycin and HU plates, but not on MBC plates, whereas the growth of *rad3Δ* and *rad26Δ* cells was compromised on all three types of medium (Fig. 5). The *rad3-gfp* cells also failed to arrest mitosis in the presence of phleomycin (Fig. 4A), confirming that they have lost the DNA-structure checkpoint. The *rad3-gfp* allele also co-segregated with sensitivity

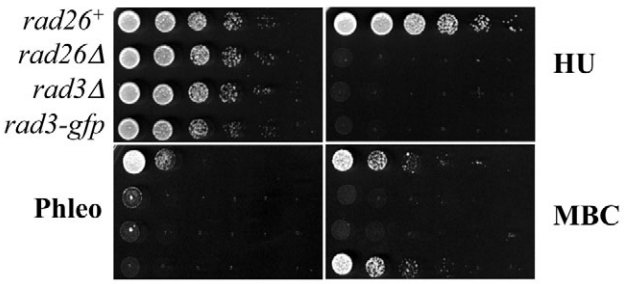

Fig. 5. The *rad3-gfp* allele also genetically separates the microtubule-damage response from the DNA-structure checkpoint response. Cultures of *rad26*$^{+}$ (TE236), *rad26Δ* (TE257), *rad3Δ* (TE570) and *rad3-gfp* (TW1203) cells were used to perform plate assays (see Materials and Methods) on YE5S (complete medium), YE5S plus 5 mM HU, YE5S plus 0.125 μg/ml phleomycin and YE5S plus 8 μg/ml MBC.

to growth on plates containing HU (data not shown). Therefore, the *rad3-gfp* allele separates the role of Rad3 during microtubule damage from its roles during genomic damage. This allele is used within the next series of experiments to help categorize phenotypes associated with the *rad26:4A* allele and concomitant loss of the Rad26-dependent response to microtubule damage.

The *rad26:4A* allele influences morphology and chromosome stability

We reported previously that *rad26Δ* and *rad3Δ* cells display morphological defects and spontaneous chromosome instability (Baschal et al., 2006). Here, we used *rad26:4A* cells (sensitive to microtubule damage but not genomic damage) and *rad3-gfp* cells (sensitive to genomic damage but not microtubule damage) to determine whether morphology and/or chromosome stability are influenced by this response to microtubule damage.

Fission yeast are rod-shaped, cylindrical cells that elongate from each end (Mitchison and Nurse, 1985). We imaged untreated cycling cells with differential interference contrast (DIC) microscopy and observed that *rad26*$^{+}$ cells were 2.53-fold longer than they were wide (L/W ratio=2.53; Fig. 6A). Similar to our previous report (Baschal et al., 2006), *rad26Δ* cells were more spherical, with a L/W ratio of 2.03. The *rad26:4A, rad3Δ* and *mad2Δ* cells shared this spherical appearance and very similar L/W ratios of 1.99, 2.05 and 2.01, respectively. By contrast, *rad3-gfp* cells retained the normal cylindrical rod shape and the wild-type L/W ratio of 2.47. We conclude that morphology is influenced by microtubule-damage responses and not by the DNA-damage response.

Fission yeast chromosome-loss assays can be performed using *ade*$^{-}$ strains that carry a genomic *ade6-210* allele (Javerzat et al., 1996). These strains are then converted to *ade*$^{+}$ strains by means of intragenic complementation with the *ade6-216* allele of a centromere-containing minichromosome. Estimates of chromosome loss are calculated by determining the number of cells that lose the minichromosome and become *ade*$^{-}$ after 40 hours of growth in complete liquid media containing adenine (Baschal et al., 2006). We observed that 0.19% of *rad26*$^{+}$ and 3.21% of *rad26Δ* cells spontaneously lost the minichromosome during the growth period (Fig. 6B), showing that *rad26*$^{+}$ prevents spontaneous minichromosome loss. The *rad26:4A* cells also lost the minichromosome at an elevated level (0.62%) that was significantly greater than that of *rad26*$^{+}$ cells but significantly less than *rad26Δ*

Table 1. Fission yeast strains

Strain number	Strain	References
TE236	*leu1-32 ura 4-d18 h*$^{-}$	(Kostrub et al., 1998)
TE257	*rad26::ura4*$^{+}$ *ade6-704 leu1-32 ura4-D18 h*$^{-}$	(Al-Khodairy et al., 1994)
TE570	*rad3::ura4*$^{+}$ *ade6-704 leu1-32 ura4-D18 h*$^{-}$	(Bentley et al., 1996)
TE787	*rad3::ura4*$^{+}$ *ade6-M210 [Ch16 ade6-216]*	Gift of Carolyn R. Chapman
TW1219	*mad2::ura4 ura4-D18 leu1-32 h*$^{-}$	(Sugimoto et al., 2004)
TW1222	*[Ch16 ade6-216] ade6-210 leu1-32 ura4-D18*	(Javerzat et al., 1996)
TW1224	*rad26::ura4*$^{+}$ *ade6-210 ura4-D18 [Ch 16 ade6-216]*	(Baschal et al., 2006)
TW1234	*rad26-yfp (G418*^{R}*) ade6-704 h–*	This study
TW1275	*rad26:4A (leu*$^{+}$*) rad26::ura4*$^{+}$ *leu1-32 ura4-D18 ade6-704 h+*	This study
TW1279	*rad26:4A-yfp (leu*$^{+}$ *G418*^{R}*) rad26::ura4*$^{+}$ *leu1-32 ura4-D18 ade6-704 h+*	This study
TW1280	*nda3-TB101 rad26::ura*$^{+}$	This study
TW1281	*rad26:4A-yfp (leu*$^{+}$ *G418*^{R}*) rad26::ura+ [Ch 16 ade6-216] ade6-210*	This study
TW1203	*rad3-gfp (G418*^{R}*) ura4-294 leu1-32 h+*	This study
TW1282	*rad3-gfp (G418*^{R}*) [Ch16 ade6-216] ade6-210*	This study
TW1285	*nda3-TB101 h+*	(Yamamoto, 1980)
TW1286	*rad26::ura*$^{+}$ *mad2::ura*$^{+}$ *ade6-210*	This study
TW1289	*rad26::ura*$^{+}$ *mad2::ura*$^{+}$ *[Ch 16 ade6-216] ade6-210*	This study
TW1290	*rad26:4A-yfp (leu*$^{+}$ *G418*^{R}*) rad26::ura*$^{+}$ *mad2::ura*$^{+}$ *[Ch 16 ade6-216] ade6-210*	This study
TW1291	*rad3-gfp mad2::ura*$^{+}$ *[Ch 16 ade6- 216] ade6-210*	This study
TW1293	*mad2::ura*$^{+}$ *[Ch 16 ade6-216] ade6-210*	This study
TW1294	*nda3-km311 ura4-D18 leu1-32 ade6-210 h–*	Dannel McCollum, UMass Medical School, MA
TW1295	*nda3-km311 rad26::ura4*$^{+}$ *ura4-D18*	This study
TW1297	*nda3-km311 mad2::ura4*$^{+}$ *ura4-D18*	This study
TW1300	*rad26::ura4*$^{+}$ *cdc25.22 cut12-egfp:ura4*$^{+}$	This study
TW1301	*nda3-km311 rad26::ura4*$^{+}$ *mad2::ura4*$^{+}$ *ura4-D18*	This study
TW1307	*cdc25.22 cut12-egfp:ura4*$^{+}$	This study
TW1308	*mad2::ura4*$^{+}$ *cdc25.22 cut12-egfp:ura4*$^{+}$	This study
TW1311	*rad26:4A-yfp (leu*$^{+}$ *G418*^{R}*) rad26::ura4*$^{+}$ *cdc25.22 cut12-egfp:ura4*$^{+}$	This study
TW1312	*rad3-gfp cdc25.22 cut12-egfp:ura4*$^{+}$	This study
TW1313	*rad26:4A-yfp (leu*$^{+}$ *G418*^{R}*) rad26::ura*$^{+}$ *rad3-gfp [Ch 16 ade6-216] ade6-210*	This study

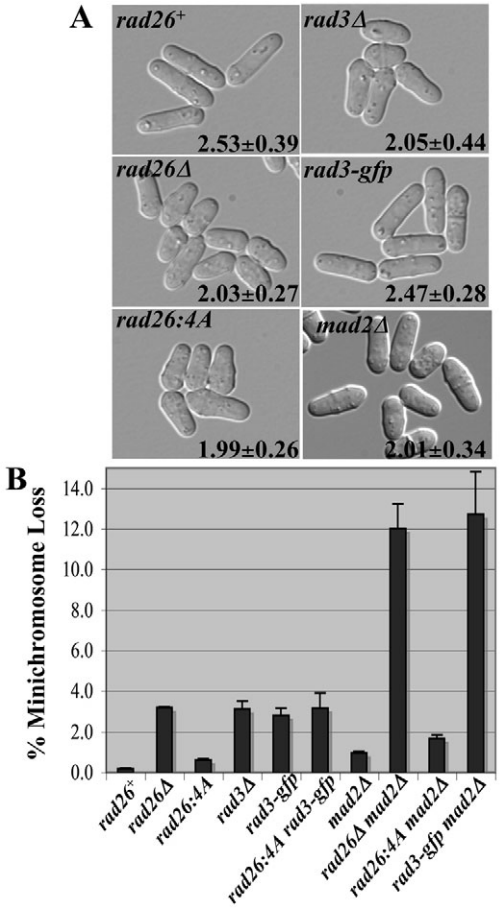

Fig. 6. The *rad26:4A* allele influences morphology and chromosome stability. (**A**) The morphology of *rad26:4A* cells was compromised. Cultures of *rad26*$^{+}$ (TE236), *rad26Δ* (TE257), *rad26:4A* (TW1275), *rad3Δ* (TE570), *rad3-gfp* (TW1203) and *mad2Δ* (TW1219) cells were grown in liquid YE5S to OD 0.3 before taking pictures. The length/width ratios indicated were acquired using Leica software (see Materials and Methods). (**B**) Minichromosome loss was elevated in *rad26:4A* cells. Cultures containing the adenine-marked minichromosome [*rad26*$^{+}$ (TW1222), *rad26Δ* (TW1224), *rad26:4A-yfp* (TW1281), *rad3Δ* (TE787), *rad3-gfp* (TW1282), *mad2Δ* (TW1293), *rad26:4A rad3-gfp* (TW1313), *rad26Δ mad2Δ* (TW1289), *rad26:4A mad2Δ* (TW1290), and *rad3-gfp mad2Δ* (TW1291)] were grown in liquid YE5S (complete medium) and then screened for minichromosome loss (see Materials and Methods).

cells (χ^2 P<0.05). We conclude that the *rad26:4A* allele defines a function that contributes slightly, but significantly, to chromosome maintenance.

Next, we used the *rad3-gfp* allele (only DNA checkpoint defective) to test whether DNA checkpoint function contributes to chromosome stability (Fig. 6B). Our results show that the minichromosome instability of *rad3-gfp* cells (2.83%) was significantly greater than that of *rad26:4A* cells (0.62%), but less than that of *rad3Δ* cells (3.12%). Minichromosome loss in the *rad3-gfp rad26:4A* double mutant (3.19%) was not significantly different from that of *rad26Δ* (3.21%) or *rad3Δ* (3.12%). Together, these data demonstrate that Rad26 and Rad3 influence spontaneous chromosome instability by at least two different mechanisms: a minor mechanism that is absent in *rad26:4A* cells and a more significant mechanism that is absent in *rad3-gfp* cells.

Lastly, we used this chromosome-loss assay to test whether Mad2 participates in either of these two chromosome-loss mechanisms (Fig. 6B). First, we observed that *mad2Δ* and *rad26:4A* produced an additive effect in which the *mad2Δrad26:4A* double mutant (1.67%) lost a chromosome amount almost identical to the sum of the single mutants (*mad2Δ*=0.96%; *rad26:4A*=0.62%). This is consistent with our conclusion that Rad26 and Mad2 operate in different pathways. Second, striking phenotypes appeared when the *mad2Δ* allele was crossed into *rad26Δ* and *rad3-gfp* backgrounds, as ⩾12% of the *mad2Δrad26Δ* and *mad2Δrad3-gfp* double mutants experienced minichromosome loss. This suggests that the spindle-assembly checkpoint and the DNA checkpoint pathways cooperate synergistically to preserve faithful chromosome transmission.

Rad26 delays mitotic entry during MBC treatment

MBC is known to inhibit late interphase events of the fission yeast cell cycle (Walker, 1982). Recently, it was reported that 75 μg/ml MBC causes a G_2 delay in fission yeast (Balestra and Jimenezk, 2008). We tested whether *rad26*$^{+}$ was required for this MBC-dependent delay using a temperature-sensitive *cdc25.22* allele that reversibly blocks cells in G_2 and the spindle-pole-body marker Cut12-EGFP to indicate mitotic entry (Fantes, 1979; Bridge et al., 1998; Craven et al., 1998). A representative G_2 cell with one Cut12-EGFP signal and a representative mitotic cell with two Cut12-EGFP foci are shown in Fig. 7.

When released to 20°C in the absence of MBC, the timing of spindle-pole-body separation was similar in *rad26*$^{+}$, *mad2Δ* and *rad3-gfp* cells, but slightly accelerated in both *rad26Δ* and *rad26:4A* cells. When released to 20°C in the presence of 16 μg/ml MBC, *rad26*$^{+}$, *mad2Δ* and *rad3-gfp* cells delayed spindle-pole-body separation for more than 180 minutes. However, *rad26Δ* and *rad26:4A* cells progressed slowly into mitosis, reaching ~50% with two Cut12 foci by 180 minutes. Therefore, the *rad26:4A* allele compromises this delay, which occurs independently of the DNA-structure and spindle-assembly checkpoints.

Discussion

We identified a conserved, hydrophobic C-terminal motif in Rad26^{ATRIP} that was shown previously to function as an NES for Lcd1^{ATRIP} in undamaged cycling cells (Jensen et al., 2000). Here, we report that this motif is also required for proper cytoplasmic localization of Rad26^{ATRIP} in undamaged cycling cells (Fig. 3). Loss of cytoplasmic Rad26^{ATRIP} by the *rad26:4A* allele accompanied phenotypes that all implicate a compromised response to microtubule damage: sensitivity to microtubule toxins; morphological abnormalities; spontaneous minichromosome segregation errors; and failure to properly delay mitosis when microtubules are damaged. Meanwhile, the DNA-damage response of these *rad26:4A* cells was preserved. In fact, these cells displayed greater resistance to phleomycin than *rad26*$^{+}$ cells (Fig. 2B), possibly due to higher concentrations of nuclear Rad26^{ATRIP} (Fig. 3). An explanation for these data is that nuclear Rad26^{ATRIP} is required when DNA is damaged and cytoplasmic Rad26^{ATRIP} is required when microtubules are damaged.

Results with budding yeast, *Drosophila melanogaster* and human cells have previously established that DNA-checkpoint proteins influence cytoplasmic responses. However, these responses depend on genomic damage. In budding yeast, DNA damage initiates a nuclearly delimited cascade of checkpoint events that delay mitosis (Demeter et al., 2000) and a cytoplasmic cascade that influences

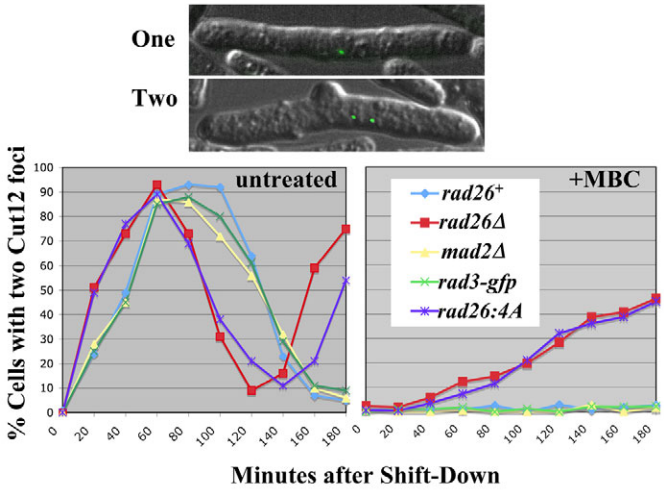

Fig. 7. An MBC-dependent G_2 delay is compromised in *rad26:4A* cells. Spindle-pole-body separation was monitored before and during MBC treatment in strains [*rad26*$^+$ (TW1307), *rad26Δ* (TW1300), *rad26:4A-yfp* (TW1311), *rad3-gfp* (TW1312) and *mad2Δ* (TW1308)] that contained the *cdc25.22* and *cut12-egfp* alleles. Cells of each strain were cultured in YE5S liquid medium to OD 0.3 at 30°C, then shifted to 37°C for 3 hours 5 minutes before 16 μg/ml MBC was added. Cultures were maintained in the presence of MBC at 37°C for another 25 minutes before downshifting to 20°C and releasing cells from the *cdc25.22* block. The percentage of cells containing two Cut12-EGFP foci was determined every 20 minutes following this downshift. Representative cells with one or two Cut12-EGFP foci are shown.

nuclear movements (Dotiwala et al., 2007). Experiments with *Drosophila* Chk2 (Takada et al., 2003) and human Chk1 (Kramer et al., 2004; Loffler et al., 2007) have established that cytoplasmically localized metazoan checkpoint proteins associate with centromeres, where they delay mitotic events during genotoxic stress. Here, we found that fission yeast Rad26^{ATRIP} possibly controls a cytoplasmic response to microtubule damage that is independent of genomic damage.

TBZ, a benzimadazole derivative that targets microtubules, is also known to inhibit late interphase events of the fission yeast cell cycle (Staron and Allard, 1964; Walker, 1982). Using 20 μg/ml TBZ, we also observed that TBZ caused fission yeast to delay spindle-pole-body separation (our unpublished data) and septation, and that both delays were independent of *rad26*$^+$ (Baschal et al., 2006). This might occur because TBZ, and not MBC, depolymerizes cortical actin and disrupts cell-polarity markers, in addition to its affects on microtubules (Sawin and Snaith, 2004). The TBZ-dependent delay to mitosis might therefore result from the activation of multiple checkpoint pathways that might or might not include the Rad26-dependent pathway discussed here.

On the mechanism of this response

A mechanism in fission yeast that delays mitotic entry in response to MBC-dependent microtubule damage during G_2 was reported recently (Balestra and Jimenez, 2008). The authors found that growth of *wee1Δ* and *cdc2-1w* cells (insensitive to Wee1 inhibition; Enoch and Nurse, 1990) was MBC sensitive, whereas growth of *cdc25Δ* and *cdc2-3w* cells (insensitive to Cdc25 activation) (Enoch and Nurse, 1990) was not. G_2-synchronized *wee1* cells also failed to delay mitosis following the addition of 75 μg/ml MBC, whereas *cdc25* cells delayed mitosis normally. Moreover, they observed that Wee1, degradation of which triggers mitosis (McGowan and Russell, 1995; Aligue et al., 1997; Muñoz et al., 1999; Watanabe et al., 2005), was stabilized in MBC-treated cells. These results show that a checkpoint mechanism responds to MBC-dependent G_2 microtubule damage by stabilizing Wee1 and delaying mitotic entry.

Many questions about this Rad26-dependent response remain. For example, does Rad26^{ATRIP} function to target and stabilize the Wee1 kinase when interphase microtubules are damaged? Does Rad26 react to physical perturbations of the microtubule cytoskeleton or a secondary consequence of microtubule damage? Do the morphological abnormalities and chromosome-segregation errors of *rad26:4A* cells arise because they enter mitosis with microtubule damage?

Morphology and chromosome segregation

Morphological abnormalities of *rad26:4A* cells might develop as these cells progress into mitosis despite the presence of interphase microtubule damage. In other words, abnormal morphology might be an indirect consequence of the checkpoint defect. However, it is possible that Rad26 directly influences morphology. For example, human ATM has been shown to specifically affect RhoA activity during the DNA-damage response and physically interact with CKIP-1, a regulator of the actin cytoskeleton (Canton et al., 2005; Frisan et al., 2003; Zhang et al., 2006).

Rad26 preserves chromosome stability by at least two different mechanisms. The more minor mechanism is defined by the *rad26:4A* allele and might result when cells enter mitosis despite the presence of damaged microtubules. The major mechanism is defined by DNA-structure checkpoint defects that probably compromise the repair of spontaneous double-strand breaks to encourage chromosome loss (reviewed by Elledge, 1996; Paulovich et al., 1997; Lengauer et al., 1998). The existence of these two mechanisms in fission yeast predicts that multiple mechanisms of chromosome loss are also present in vertebrate DNA-checkpoint-defective cells.

Conclusion

Fission yeast use the Rad26-dependent response when microtubules are damaged in G_2 and the Mad2-dependent response when microtubules are damaged in mitosis. These pathways cooperate to influence the fidelity of chromosome segregation, which suffers in an additive fashion following loss of both pathways (Fig. 6). Crosstalk between the pathways was not readily apparent, because Rad26 was not required for the Mad2-dependent response and vice versa (Figs 1 and 7). The questions of what this Rad26-dependent checkpoint pathway responds to and how it delays mitosis remain.

Materials and Methods

Strains, growth conditions and chemical stock solutions

The strains used in this study were grown under standard conditions (Moreno et al., 1991), unless noted otherwise (Table 1). Chemical reagents and stock solutions are as follows: MBC (Sigma, St Louis, MO, USA) was stored as an 8 mg/ml DMSO solution; phleomycin (Research Products International, Mt Prospect, IL, USA) as a 5 mg/ml DMSO solution; and HU (Sigma) as a 200 mM H_2O solution.

Physiological methods

To perform plate assays, cultures grown to an optical density (OD) of 0.3 in YE5S liquid medium were serially diluted by a factor of 5. From each dilution, 5 μl aliquots were manually spotted onto plates using a Pipetman. Spot assays were repeated twice with similar results.

Minichromosome stability assays were performed using cells cultured in YE5S liquid medium for 40 hours to OD 0.5. Cultures were then diluted and plated in YE5S medium for 2 days at 30°C. Colonies were then replica plated to EMM

minimal media lacking adenine (EMM–adenine) for 2 days at 30°C. Dark red colonies unable to grow well on these EMM–adenine plates had lost the minichromosome. Three trials were performed and 200 cells were scored per trial.

Spindle-pole-body separation was monitored in different strains containing *cdc25.22* and *cut12-egfp*. Cells of each strain were cultured in YE5S liquid medium to OD 0.3 at 30°C, then shifted to 37°C for 3 hours 5 minutes before 16 μg/ml MBC was added. Cultures were maintained in the presence of MBC at 37°C for another 25 minutes before downshifting to ~20°C and releasing cells from the *cdc25.22* block. The percentage of cells containing two Cut12-EGFP foci or a septum was determined every 20 minutes following this downshift. Three trials were performed and 200 cells were scored at every 20 minute time point.

Flow cytometry and *nda3-km311* experiments were used to investigate spindle-assembly checkpoint integrity. Flow cytometry experiments were performed using cells cultured in YE5S liquid medium to OD 0.3. Cultures were then treated with MBC (8 μg/ml) and 1 ml aliquots were collected every hour for four hours and processed according to the procedure found on the Forsburg laboratory web site (www-rcf.usc.edu/~forsburg/yeast-flow-protocol.html). Briefly, cells were fixed in 70% ethanol and washed with 50 mM sodium citrate before treating with RNase and staining with Sytox Green (Molecular Probes, Eugene, OR, USA). Flow analysis was performed using a Coulter Elite Epics flow cytometer. Strains carrying the cold-sensitive *nda3-km311* allele were cultured at 30°C in YE5S liquid medium to OD 0.3 before downshifting to 20°C for 5 hours. The cells were then fixed in cold methanol and stained with DAPI (Sigma) to observe chromatin and calcofluor (Sigma) to stain septa. Images were captured using a Leica DM5000 equipped with a Leica DFC350FX R2 digital camera and Leica FW4000 software. The percentage of cells containing condensed chromatin was measured using data acquired from two independent trials in which the number of cells containing condensed chromatin was determined for 200 cells.

Microscopy, L/W ratios and fluorescence intensity measurements

For DIC microscopy, cells were imaged directly from cultures grown in liquid YE5S to OD 0.3. To visualize EGFP and YFP fusion proteins, 1 ml aliquots from cultures grown in liquid YE5S to OD 0.3 were centrifuged and resuspended in cold methanol for one minute, washed twice in 100 μl *SlowFade* Component C (*SlowFade* Antifade Kit, Molecular Probes) and air dried on coverglass (Fisher). Once dried, 4.5 μl *SlowFade* Component A was dropped on the coverglass, which was then placed onto a slide. Achieving yeast monolayers that adhered tightly to the coverslips was crucial to observing YFP signals. To help ensure that such layers formed, the coverglass was soaked in acetone for one day, scrubbed with dishwashing soap, wiped with 70% ethanol (Sigma) and air dried prior to use. When compared with live cells expressing YFP fusions, methanol fixation did not affect the localization of YFP signals, but greatly facilitated formation of adherent monolayers (data not shown). Images were acquired using a Leica DM5000 equipped with a Leica DFC350FX R2 digital camera and Leica FW4000 software. All YFP fluorescence images were acquired with 10 second exposure times, and the contrast and brightness parameters of these images were corrected identically.

To calculate length/width (L/W) ratios, Leica software was used to acquire DIC images and measure the length and width of 100 cells. The reported L/W ratios represent the average L/W ratio calculated from two independent experiments.

Fluorescence intensity measurements were calculated using ImageJ (rsbweb.nih.gov/ij/). The data in Fig. 3B represent the relative YFP intensities derived by averaging fluorescence measurements from 50 cells of each strain.

Construction of rad26:4A, rad26-yfp, rad26:4A-yfp and rad3-gfp strains

An ~3 kb genomic *Pst*I-*Bam*HI fragment containing the *rad26*$^+$ locus cloned into pBSK+ (pTW910) vector was mutagenized using the QuikChange site-directed mutagenesis kit (Stratagene). Briefly, four hydrophobic residues within the C-terminal motif were changed to alanines (Fig. 2A) using the mutagenic primer 5′ CCCTCAAAATGAATGCGTAGAGATTTTAGTATCTGCTGCTCGGGCTGCGTA-CATTTTATCTTCCGAAGATTTATCATC 3′. The mutagenized *Pst*I-*Bam*HI fragment containing the *rad26:4A* allele was then cloned into pJK148, a *leu*$^+$ integration vector (Keeney and Boeke, 1994). The resulting vector (pTW919) was linearized at the *leu*$^+$ marker using *Eco*NI and transformed into the *rad26Δ leu1-32* fission yeast strain TE257. Of 20 *leu*$^+$ transformants selected, 100% displayed wild-type sensitivities to the genotoxic agents HU and phleomycin, and *rad26Δ* sensitivity to MBC (data not shown). We arbitrarily chose one of these strains to use in the experiments presented here (TW1275), backcrosses with which showed that the phenotypes described above (sensitivity to MBC, but not HU or phleomycin) co-segregated with *leu*$^+$ (data not shown).

Rad26 and Rad26:4A were C-terminally tagged with YFP using the technique of Bahler et al. (Bahler et al., 1998). Briefly, two primers (pRad26 forward: 5′TATTTTCTCACTACAGAATTGTTGGAAGTTTGCGTCTCTCCCGAAGAGC-TGGAGCAGTTGTACACTAATTTTCGGATCCCCGGGTTATTAA 3′; pRad26 reverse: 5′GATGTGGGTGCGGGACGGGAAAGAACAACACTGAAGAAACA-AGTATCATTATTTCATTTGAAAAATTAGGGAAATGAATTCGAGCTCGTTTA-AAC 3′) were used to amplify a YFP-kanMX6 module (gift of Dave Kovar, University of Chicago, IL, USA) using the high-fidelity polymerase Accuzyme (Bioline, Randolph, MA, USA). The resulting PCR fragment directed integration of *yfp* to the 3′ end of *rad26*$^+$ following yeast transformation, and both *rad26*$^+$ and *rad26:4A* were tagged with *yfp* in this manner. Similarly, Rad3 was C-terminally tagged with GFP using primers (pRad3 forward: 5′CAAGAATTGATCA-AATCTGCTGTCAACCCAAAAAACCTGGTAGAAATGTACATTGGTTGGGCT-GCTTATTTCCGGATCCCCGGGTTAATTAA 3′; pRad3 reverse: 5′ AATTCT-TCATCGGATTAATAAATAAAATATCTTCGATTCAAATCATAAGTTTAATAAT-GGGTAGCTTGTTCATTGGAATTCGAGCTCGTTTAAAC 3′) to amplify the GFP (S65T)-kanMX6 module of pFA6a-GFP (Bahler et al., 1998).

We thank Dan McCollum, Dave Kovar, Hiroshi Murakami, Ian Hagan and the Japanese Yeast Genetic Resource Center National BioResource Project (YGRC-NBRP) for strains and plasmids. We also thank Zach Krych and members of the Sclafani, McIntosh and Forsburg laboratories for helpful suggestions and technical assistance. This work was supported by UCHSC and an American Cancer Society institutional research grant (57-001-47), a National Science Foundation Major Research Initiative equipment grant (4540122) and a UCCS CRCW award.

References

Abraham, R. T. (2001). Cell cycle checkpoint signaling through the ATM and ATR kinases. *Genes Dev.* **15**, 2177-2196.

Aligue, R., Wu, L. and Russell, P. (1997). Regulation of *Schizosaccharomyces pombe* Wee1 tyrosine kinase. *J. Biol. Chem.* **272**, 13320-13325.

Al-Khodairy, F. and Carr, A. M. (1992). DNA repair mutants defining G2 checkpoint pathways in *Schizosaccharomyces pombe*. *EMBO J.* **11**, 1343-1350.

Al-Khodairy, F., Fotou, E., Sheldrick, K. S., Griffiths, D. J., Lehmann, A. R. and Carr, A. M. (1994). Identification and characterization of new elements involved in checkpoint and feedback controls in fission yeast. *Mol. Biol. Cell* **5**, 147-160.

Bahler, J., Wu, J. Q., Longtine, M. S., Shah, N. G., Mckenzie, A. R., Steever, A. B., Wach, A., Philippsen, P. and Pringle, J. R. (1998). Heterologous modules for efficient and versatile PCR-based gene targeting in *Schizosaccharomyces pombe*. *Yeast* **14**, 943-951.

Balestra, F. R. and Jimenez, J. (2008). A G2-Phase microtubule-damage response in fission yeast. *Genetics* **180**, 2073-2080.

Balla, S., Thapar, V., Verma, S., Luong, T., Faghri, T., Huang, C. H., Rajasekaran, S., Del Campo, J. J., Shinn, J. H., Mohler, W. A. et al. (2006). Minimotif Miner: a tool for investigating protein function. *Nat. Methods* **3**, 175-177.

Bartkova, J., Horejsi, Z., Koed, K., Kramer, A., Tort, F., Zieger, K., Guldberg, P., Sehested, M., Nesland, J. M., Lukas, C. et al. (2005). DNA damage response as a candidate anti-cancer barrier in early human tumorigenesis. *Nature* **434**, 864-870.

Baschal, E. E., Chen, K. J., Elliott, L. G., Herring, M. J., Verde, S. C. and Wolkow, T. D. (2006). The fission yeast DNA structure checkpoint protein Rad26 responds to microtubule stress. *BMC Cell Biol.* **7**, 32.

Bentley, N. J., Holtzman, D. A., Flaggs, G., Keegan, K. S., Demaggio, A., Ford, J. C., Hoekstra, M. and Carr, A. M. (1996). The *Schizosaccharomyces pombe rad3* checkpoint gene. *EMBO J.* **15**, 6641-6651.

Bridge, A. J., Morphew, M., Bartlett, R. and Hagan, I. M. (1998). The fission yeast SPB component Cut12 links bipolar spindle formation to mitotic control. *Genes Dev.* **12**, 927-942.

Bonilla, C. Y., Melo, J. A. and Toczyski, D. P. (2008). Colocalization of sensors is sufficient to activate the DNA damage checkpoint in the absence of damage. *Mol. Cell* **30**, 267-276.

Canton, D. A., Olsten, M. E., Kim, K., Doherty-Kirby, A., Lajoie, G., Cooper, J. A. and Litchfield, D. W. (2005). The pleckstrin homology domain-containing protein CKIP-1 is involved in regulation of cell morphology and the actin cytoskeleton and interaction with actin capping protein. *Mol. Cell. Biol.* **25**, 3519-3534.

Carr, A. M. (1995). DNA structure checkpoints in fission yeast. *Semin. Cell Biol.* **6**, 65-72.

Clemenson, C. and Marsolier-Kergoat, M. C. (2006). The spindle assembly checkpoint regulates the phosphorylation state of a subset of DNA checkpoint proteins in *Saccharomyces cerevisiae*. *Mol. Cell. Biol.* **26**, 9149-9161.

Collura, A., Blaisonneau, J., Baldacci, G. and Francesconi, S. (2005). The fission yeast Crb2/Chk1 pathway coordinates the DNA damage and spindle checkpoint in response to replication stress induced by topoisomerase I inhibitor. *Mol. Cell. Biol.* **25**, 7889-7899.

Cortez, D., Guntuku, S., Qin, J. and Elledge, S. J. (2001). ATR and ATRIP: partners in checkpoint signaling. *Science* **294**, 1713-1716.

Craven, R. A., Griffiths, D. J., Sheldrick, K. S., Randall, R. E., Hagan, I. M. and Carr, A. M. (1998). Vectors for the expression of tagged proteins in *Schizosaccharomyces pombe*. *Gene* **221**, 59-68.

De Souza, C. P., Ye, X. S. and Osmani, S. A. (1999). Checkpoint defects leading to premature mitosis also cause endoreplication of DNA in *Aspergillus nidulans*. *Mol. Biol. Cell* **10**, 3661-3674.

Demeter, J., Lee, S. E., Haber, J. E. and Stearns, T. (2000). The DNA damage checkpoint signal in budding yeast is nuclear limited. *Mol. Cell* **6**, 487-492.

Dotiwala, F., Haase, J., Arbel-Eden, A., Bloom, K. and Haber, J. E. (2007). The yeast DNA damage checkpoint proteins control a cytoplasmic response to DNA damage. *Proc. Natl. Acad. Sci. USA* **104**, 11358-11363.

Edwards, R. J., Bentley, N. J. and Carr, A. M. (1999). A Rad3-Rad26 complex responds to DNA damage independently of other checkpoint proteins. *Nat. Cell Biol.* **1**, 393-398.

Elledge, S. J. (1996). Cell cycle checkpoints: preventing an identity crisis. *Science* **274**, 1664-1672.
Enoch, T. and Nurse, P. (1990). Mutation of fission yeast cell cycle control genes abolishes dependence of mitosis on DNA replication. *Cell* **60**, 665-673.
Enoch, T., Carr, A. M. and Nurse, P. (1992). Fission yeast genes involved in coupling mitosis to completion of DNA replication. *Genes Dev.* **6**, 2035-2046.
Enserink, J. M., Smolka, M. J., Zhou, H. and Kolodner, R. D. (2006). Checkpoint proteins control morphogenetic events during DNA replication stress in *Saccharomyces cerevisiae*. *J. Cell Biol.* **175**, 729-741.
Fantes, P. A. (1979). Epistatic gene interactions in the control of division in fission yeast. *Nature* **279**, 428-430.
Frisan, T., Cortes-Bratti, X., Chaves-Olarte, E., Stenerlow, B. and Thelestam, M. (2003). The Haemophilus ducreyi cytolethal distending toxin induces DNA double-strand breaks and promotes ATM-dependent activation of RhoA. *Cell. Microbiol.* **5**, 695-707.
Garber, P. M. and Rine, J. (2002). Overlapping roles of the spindle assembly and DNA damage checkpoints in the cell-cycle response to altered chromosomes in *Saccharomyces cerevisiae*. *Genetics* **161**, 521-534.
Hartwell, L. (1992). Defects in a cell cycle checkpoint may be responsible for the genomic instability of cancer cells. *Cell* **71**, 543-546.
Hartwell, L. H. and Weinert, T. A. (1989). Checkpoints: controls that ensure the order of cell cycle events. *Science* **246**, 629-634.
He, X., Patterson, T. E. and Sazer, S. (1997). The *Schizosaccharomyces pombe* spindle checkpoint protein Mad2p blocks anaphase and genetically interacts with the anaphase-promoting complex. *Proc. Natl. Acad. Sci. USA* **94**, 7965-7970.
Jacobs, C. W., Adams, A. E., Szaniszlo, P. J. and Pringle, J. R. (1988). Functions of microtubules in the *Saccharomyces cerevisiae* cell cycle. *J. Cell Biol.* **107**, 1409-1426.
Javerzat, J. P., Cranston, G. and Allshire, R. C. (1996). Fission yeast genes which disrupt mitotic chromosome segregation when overexpressed. *Nucleic Acids Res.* **24**, 4676-4683.
Jensen, T. H., Neville, M., Rain, J. C., McCarthy, T., Legrain, P. and Rosbash, M. (2000). Identification of novel *Saccharomyces cerevisiae* proteins with nuclear export activity: cell cycle-regulated transcription factor ace2p shows cell cycle-independent nucleocytoplasmic shuttling. *Mol. Cell. Biol.* **20**, 8047-8058.
Kanbe, T., Hiraoka, Y., Tanaka, K. and Yanagida, M. (1990). The transition of cells of the fission yeast beta-tubulin mutant *nda3-311* as seen by freeze-substitution electron microscopy. Requirement of functional tubulin for spindle pole body duplication. *J. Cell Sci.* **96**, 275-282.
Kastan, M. B. and Bartek, J. (2004). Cell-cycle checkpoints and cancer. *Nature* **432**, 316-323.
Keeney, J. B. and Boeke, J. D. (1994). Efficient targeted integration at leu1-32 and ura4-294 in *Schizosaccharomyces pombe*. *Genetics* **136**, 849-856.
Keith, C. T. and Schreiber, S. L. (1995). PIK-related kinases: DNA repair, recombination, and cell cycle checkpoints. *Science* **270**, 50-51.
Kostrub, C. F., Knudsen, K., Subramani, S. and Enoch, T. (1998). Hus1p, a conserved fission yeast checkpoint protein, interacts with Rad1p and is phosphorylated in response to DNA damage. *EMBO J.* **17**, 2055-2066.
Kramer, A., Mailand, N., Lukas, C., Syljuasen, R. G., Wilkinson, C. J., Nigg, E. A., Bartek, J. and Lukas, J. (2004). Centrosome-associated Chk1 prevents premature activation of cyclin-B-Cdk1 kinase. *Nat. Cell Biol.* **6**, 884-891.
Krishnan, V., Nirantar, S., Crasta, K., Cheng, A. Y. and Surana, U. (2004). DNA replication checkpoint prevents precocious chromosome segregation by regulating spindle behavior. *Mol. Cell* **16**, 687-700.
Kutay, U. and Guttinger, S. (2005). Leucine-rich nuclear-export signals: born to be weak. *Trends Cell Biol.* **15**, 121-124.
Larkin, M. A., Blackshields, G., Brown, N. P., Chenna, R., McGettigan, P. A., McWilliam, H., Valentin, F., Wallace, I. M., Wilm, A., Lopez, R. et al. (2007). Clustal W and Clustal X version 2.0. *Bioinformatics* **23**, 2947-2948.
Lengauer, C., Kinzler, K. W. and Vogelstein, B. (1998). Genetic instabilities in human cancers. *Nature* **396**, 643-649.
Li, R. and Murray, A. W. (1991). Feedback control of mitosis in budding yeast. *Cell* **66**, 519-531.
Loffler, H., Bochtler, T., Fritz, B., Tews, B., Ho, A. D., Lukas, J., Bartek, J. and Kramer, A. (2007). DNA damage-induced accumulation of centrosomal Chk1 contributes to its checkpoint function. *Cell Cycle* **6**, 2541-2548.
Malavazi, I., Semighini, C. P., Kress, M. R., Harris, S. D. and Goldman, G. H. (2006). Regulation of hyphal morphogenesis and the DNA damage response by the *Aspergillus nidulans* ATM homolog *AtmA*. *Genetics* **173**, 99-109.
McGowan, C. H. and Russell, P. (1995). Cell cycle regulation of human WEE1. *EMBO J.* **14**, 2166-2175.
Mckinnon, P. J. and Burgoyne, L. A. (1985). Altered cellular morphology and microfilament array in *ataxia-telangiectasia* fibroblasts. *Eur. J. Cell Biol.* **39**, 161-166.
Melo, J. and Toczyski, D. (2002). A unified view of the DNA-damage checkpoint. *Curr. Opin. Cell Biol.* **14**, 237-245.
Mikhailov, A., Cole, R. W. and Rieder, C. L. (2002). DNA damage during mitosis in human cells delays the metaphase/anaphase transition via the spindle-assembly checkpoint. *Curr. Biol.* **12**, 1797-1806.
Mitchison, J. M. and Nurse, P. (1985). Growth in cell length in the fission yeast *Schizosaccharomyces pombe*. *J. Cell Sci.* **75**, 357-376.
Moreno, S., Klar, A. and Nurse, P. (1991). Molecular genetic analysis of fission yeast *Schizosaccharomyces pombe*. *Methods Enzymol.* **194**, 795-823.
Muñoz, M. J., Bejarano, E. R., Daga, R. R. and Jimenez, J. (1999). The identification ofWos2, a p23 homologue that interacts withWee1 and Cdc2 in the mitotic control of fission yeasts. *Genetics* **153**, 1561-1572.
Opperman, T., Murli, S., Smith, B. T. and Walker, G. C. (1999). A model for a umuDC-dependent prokaryotic DNA damage checkpoint. *Proc. Natl. Acad. Sci. USA* **96**, 9218-9223.
Paciotti, V., Clerici, M., Lucchini, G. and Longhese, M. P. (2000). The checkpoint protein Ddc2, functionally related to *S. pombe* Rad26, interacts with Mec1 and is regulated by Mec1-dependent phosphorylation in budding yeast. *Genes Dev.* **14**, 2046-2059.
Paulovich, A. G., Toczyski, D. P. and Hartwell, L. H. (1997). When checkpoints fail. *Cell* **88**, 315-321.
Rouse, J. and Jackson, S. P. (2002a). Lcd1p recruits Mec1p to DNA lesions *in vitro* and *in vivo*. *Mol. Cell* **9**, 857-869.
Rouse, J. and Jackson, S. P. (2002b). Interfaces between the detection, signaling, and repair of DNA damage. *Science* **297**, 547-551.
Rowley, R., Subramani, S. and Young, P. G. (1992). Checkpoint controls in *Schizosaccharomyces pombe: rad1*. *EMBO J.* **11**, 1335-1342.
Sawin, K. and Snaith, H. (2004). Role of microtubules and tea1p in establishment and maintenance of fission yeast cell polarity. *J. Cell Sci.* **117**, 689-700.
Sczaniecka, M., Feoktistova, A., May, K. M., Chen, J. S., Blyth, J., Gould, K. L. and Hardwick, K. G. (2008). The spindle checkpoint functions of Mad3 and Mad2 depend on a Mad3 KEN box-mediated interaction with Cdc20-anaphase-promoting complex (APC/C). *J. Biol. Chem.* **283**, 23039-23047.
Sleigh, M. J. and Grigg, G. W. (1977). Sulphydryl-mediated DNA breakage by phlemomycin in *Escherichia coli*. *Mutat. Res.* **42**, 181-190.
Staron, T. and Allard, C. (1964). Propri6t6s anti-fongiques du 2-(4′-thiazolyl) benzimidazole ou thiabendazole. *Phytiatr.-Phytopharm. Rev. Ft. Med. Pharm. Veg.* **13**, 163.
Sugimoto, I., Murakami, H., Tonami, Y., Moriyama, A. and Nakanishi, M. (2004). DNA replication checkpoint control mediated by the spindle checkpoint protein Mad2p in fission yeast. *J. Biol. Chem.* **279**, 47372-47378.
Takada, S., Kelkar, A. and Theurkauf, W. E. (2003). Drosophila checkpoint kinase 2 couples centrosome function and spindle assembly to genomic integrity. *Cell* **113**, 87-99.
Umesono, K., Toda, T., Hayashi, S. and Yanagida, M. (1983). Cell division cycle genes *nda2* and *nda3* of the fission yeast *Schizosaccharomyces pombe* control microtubular organization and sensitivity to anti-mitotic benzimidazole compounds. *J. Mol. Biol.* **168**, 271-284.
Wakayama, T., Kondo, T., Ando, S., Matsumoto, K. and Sugimoto, K. (2001). Pie1, a protein interacting with Mec1, controls cell growth and checkpoint responses in *Saccharomyces cerevisiae*. *Mol. Cell. Biol.* **21**, 755-764.
Walker, G. M. (1982). Cell cycle specificity of certain antimicrotubular drugs in *Schizosaccharomyces pombe*. *J. Gen. Microbiol.* **128**, 61-71.
Walworth, N., Davey, S. and Beach, D. (1993). Fission yeast Chk1 protein kinase links the *rad* checkpoint pathway to Cdc2. *Nature* **363**, 368-371.
Watanabe, N., Arai, H., Iwasaki, J., Shiina, M., Ogata, K., Hunter, T. and Osada, H. (2005). Cyclin-dependent kinase (CDK) phosphorylation destabilizes somatic Wee1 via multiple pathways. *Proc. Natl. Acad. Sci. USA* **102**, 11663-11668.
Weinert, T. A. and Hartwell, L. H. (1988). The RAD9 gene controls the cell cycle response to DNA damage in *Saccharomyces cerevisiae*. *Science* **241**, 317-322.
Weinert, T. A. and Lydall, D. (1993). Cell cycle checkpoints, genetic instability and cancer. *Semin. Cancer Biol.* **4**, 129-140.
Weinert, T. A., Kiser, G. L. and Hartwell, L. H. (1994). Mitotic checkpoint genes in budding yeast and the dependence of mitosis on DNA replication and repair. *Genes Dev.* **8**, 652-665.
Wolkow, T. D. and Enoch, T. (2002). Fission yeast Rad26 is a regulatory subunit of the Rad3 checkpoint kinase. *Mol. Biol. Cell* **13**, 480-492.
Wolkow, T. D. and Enoch, T. (2003). Fission yeast Rad26 responds to DNA damage independently of Rad3. *BMC Genet.* **4**, 6.
Yamamoto, M. (1980). Genetic analysis of resistant mutants to antimitotic benzimidazole compounds in *Schizosaccharomyces pombe*. *Mol. Gen. Genet.* **180**, 231-234.
Zachos, G. and Gillespie, D. A. (2007). Exercising restraints: role of Chk1 in regulating the onset and progression of unperturbed mitosis in vertebrate cells. *Cell Cycle* **6**, 810-813.
Zachos, G., Black, E. J., Walker, M., Scott, M. T., Vagnarelli, P., Earnshaw, W. C. and Gillespie, D. A. (2007). Chk1 is required for spindle checkpoint function. *Dev. Cell* **12**, 247-260.
Zhang, L., Tie, Y., Tian, C., Xing, G., Song, Y., Zhu, Y., Sun, Z. and He, F. (2006). CKIP-1 recruits nuclear ATM partially to the plasma membrane through interaction with ATM. *Cell. Signal.* **18**, 1386-1395.
Zhao, X., Muller, E. G. and Rothstein, R. (1998). A suppressor of two essential checkpoint genes identifies a novel protein that negatively affects dNTP pools. *Mol. Cell* **2**, 329-340.